Sequence Determination of Reduction Potentials by Cysteinyl Hydrogen Bonds and Peptide Dipoles in [4Fe-4S] Ferredoxins

Brian W. Beck, Qian Xie, and Toshiko Ichiye
Department of Biochemistry and Biophysics, School of Molecular Biosciences, Washington State University, Pullman, Washington 99164 USA

ABSTRACT A sequence determinant of reduction potentials is reported for bacterial [4Fe-4S]-type ferredoxins. The residue that is four residues C-terminal to the fourth ligand of either cluster is generally an alanine or a cysteine. In five experimental ferredoxin structures, the cysteine has the same structural orientation relative to the nearest cluster, which is stabilized by the SH···S bond. Although such bonds are generally considered weak, indications that Fe-S redox site sulfurs are better hydrogen-bond acceptors than most sulfurs include the numerous amide NH···S bonds noted by Adman and our quantum mechanical calculations. Furthermore, electrostatic potential calculations of 11 experimental ferredoxin structures indicate that the extra cysteine decreases the reduction potential relative to an alanine by ~60 mV, in agreement with experimental mutational studies. Moreover, the decrease in potential is due to a shift in the polar backbone stabilized by the SH···S bond rather than to the slightly polar cysteinyl side chain. Thus, these cysteines can "tune" the reduction potential, which could optimize electron flow in an electron transport chain. More generally, hydrogen bonds involving sulfur can be important in protein structure/function, and mutations causing polar backbone shifts can alter electrostatics and thus affect redox properties or even enzymatic activity of a protein.

INTRODUCTION

The [4Fe-4S]-type ferredoxins (Fd), which are small (6–12 kDa) electron transport proteins found in bacteria (Matsubara and Saeki, 1992), contain one or two cubane-like [4Fe-4S] and/or [3Fe-4S] clusters that are usually ligated to the protein by cysteines. The [4Fe-4S] clusters have characteristically low reduction potentials that range from −645 to 0 mV (Cammack, 1992) for the $Fe_4S_4(SR)_4^{2-/3-}$ couple (Holm, 1992) whereas the [3Fe-4S] clusters have somewhat higher reduction potentials that range from −420 to −50 mV (Cammack, 1992) for the $Fe_3S_4(SR)_3^{2-/3-}$ couple (Holm, 1992). Identifying the sequence determinants that lead to the range in potentials for the same cluster is crucial in understanding the function of these proteins.

The crystal structures of the ferredoxins from *Peptostreptococcus asaccharolyticus* (Backes et al., 1991), *Chromatium vinosum* (Moulis et al., 1996), *Bacillus schlegelii* (Aono et al., 1998), *Azotobacter vinelandii* (Stout, 1993), and *Desulfovibrio africanus* (Séry et al., 1994) all have an extra cysteine whose sulfur is close to a redox site sulfur but is not ligated to an iron. This extra cysteine does not appear to perturb the cluster geometry or to form disulfide bonds (Stout, 1993; Iismaa et al., 1991). Moreover, it is unlikely to be a crystal-packing artifact because the proteins were crystallized under different conditions. Interestingly, these extra cysteines all occur four residues C-terminal to the fourth cysteinyl ligand Cys^4 of the ligation pattern Cys^1-X_2-Cys^2-X_2-Cys^3-X_n-Cys^4-Pro-X_2-Cys^x, where the *n* indicates that the fourth ligand is far removed (either upstream or downstream) in sequence from the first three (Matsubara and Saeki, 1992) and Cys^x indicates the residue position of this extra cysteine. Three are near cluster 2 and one is near cluster 1, but these may all be considered to be in equivalent locations because the two-cluster ferredoxins have a quasi twofold rotationally symmetric structure (Adman et al., 1973; Fukuyama et al., 1988; Howard and Rees, 1991) with two such ligation patterns. We propose that the extra cysteine may be involved in an SH···S hydrogen bond to the redox site and that this cysteine can alter the electrostatic potential at the redox site and thus the reduction potential of the protein.

Although sulfurs are generally considered weak hydrogen bond donors and acceptors (Voet and Voet, 1990), our recent ab initio quantum mechanical calculations have shown that the Fe-ligated sulfurs of $[Fe(SCH_3)_4]^{1-/2-}$ are better hydrogen-bond acceptors than non-metal-ligated sulfurs (Koerner and Ichiye, 2000; Beck, 1997). Other indications are the numerous NH···S hydrogen bonds involving amides and Fe-ligated sulfurs found in Fe-S proteins (Adman et al., 1975) and tritium and deuterium exchange studies indicating that the stability of these NH···S bonds is similar to that of NH···O bonds (Hong and Rabinowitz, 1970; Crespi et al., 1974). Furthermore, the larger number of NH···S bonds in the [4Fe-4S] ferredoxins than in the high-potential iron-sulfur proteins (HiPIPs) was suggested to alter their reduction potentials (Adman et al., 1975; Backes et al., 1991), although the number of NH···S bonds

Received for publication 16 November 2000 and in final form 24 April 2001.

B. W. Beck's current address: Institute for Molecular Design, University of Houston, Houston, TX 77204-5641.

Q. Xie's current address: R.O.W. Sciences, Inc., National Center for Toxicology Research, FDA, 3900 NCTR Road, Mail Code 910, Jefferson, AR 72079.

Address reprint requests to Dr. Toshiko Ichiye, Department of Biochemistry and Biophysics, Washington State University, Pullman, WA 99164-4660. Tel.: 509-335-7600; Fax: 509-335-9688; E-mail: ichiye@wsu.edu.

0006-3495/01/08/601/13 $2.00

did not correlate with reduction potential differences within a set of homologous proteins (Backes et al., 1991). Because hydrogen bonds involving sulfurs are often ignored, the identification of an SH···S hydrogen bond has important implications for sulfurs in protein structure/function studies in general.

Putative SH···S hydrogen bonds are relevant because of the numerous examples of extra cysteines. Recently, extra cysteines near cluster 1 at the Cys^x position as well as one or two residues further from Cys^4 have been noted in sequences of photosynthetic bacterial and *nif*-associated 2[4Fe-4S] ferredoxins (Saeki et al., 1996). The extra cysteines at the other positions are likely to have different interactions, although no three-dimensional structures exist for these ferredoxins. Also, extra cysteines at the Cys^x position have been found in ~20% of almost 100 bacterial ferredoxin sequences, with the remainder predominantly alanine (Q. Xie and T. Ichiye, unpublished results), indicating that the cysteine is not a silent mutation. Finally, there is a strictly conserved extra cysteine at a very different residue position in the 2[4Fe-4S] psaC protein in photosystem I (PSI) (Bryant, 1992), which is homologous to the bacterial ferredoxins (Golbeck, 1993a,b). Unfortunately, the interactions of extra cysteine cannot be characterized in the 4-Å resolution structure of the PSI complex (Krauss et al., 1996; Klukas et al., 1999).

The extra cysteines may also play a role in the energetics of electron transfer in ferredoxins. Interestingly, the mutation in *Rhizobium meliloti* FdxN of the extra cysteine to a serine at the Cys^x+2 position abolishes nitrogen fixation (Masepohl et al., 1992), whereas the analogous mutation at the Cys^x+1 position in *Rhodobacter capsulatus* FdxN has almost no effect (Saeki et al., 1996). Moreover, site-specific mutagenesis in *A. vinelandii* (Iismaa et al., 1991) and *Pyrococcus furious* (Brereton et al., 1998) ferredoxins demonstrates that a cysteine at the Cys^x position leads to a decrease in reduction potential of ~50 mV relative to an alanine at this position. Thus, an extra cysteine could serve as a tuning mechanism for the reduction potential. In an electron transport chain, the magnitude of the tuning must take into account both the energetics of electron transfer from the donor to the "tuned" protein and from the "tuned" protein to the next acceptor so that the flow at one step is optimized while favorable flow at the other step is maintained. Although electron transport chains may be able to tolerate some unfavorable transfers (Page et al., 1999), the overall driving force must favor transfer. Moreover, although the change in the reduction potential due to the cysteine is small, our research indicates that large differences in reduction potential found between homologous proteins are often due to several changes on the order of 50–100 mV each (Ichiye, 1999).

Overall, understanding the structural origins of sequence determinants of reduction potentials of proteins is difficult because the reduction potential has many contributions, including the intrinsic energy of the redox site reduction and the extrinsic energy of the environmental response to the charge change (Ichiye, 1999). Perturbations of the redox site may play a role in changing the intrinsic energy; however, these perturbations are rare for iron-sulfur sites so the focus has been on the extrinsic energy (Sweeney and Rabinowitz, 1980). The electrostatic energy is one of the largest contributors to the extrinsic energy change upon reduction and has been successfully used to understand protein reduction potentials (Stephens et al., 1996; Swartz et al., 1996; Ichiye, 1999; Gunner and Honig, 1991). For example, a decrease in the accessibility and thus electrostatic contribution of the solvent due to the addition of an entire extra helix in *A. vinelandii* ferredoxin apparently leads to a 220-mV decrease in reduction potential relative to *P. asaccharolyticus* ferredoxin (Backes et al., 1991; Jensen et al., 1994). Also, in an unusually large change caused by a single site mutation, the electrostatic contribution of an additional water in a surface pocket created in the P80A mutant of *Alcaligenes faecalis* pseudoazurin apparently leads to a 409-mV increase over wild-type (Nishiyama et al., 1992; Libeu et al., 1997). For the case studied here, previous electrostatic energy calculations by two different methods of *A. vinelandii* ferredoxin predict that the wild type with a cysteine at the Cys^x position has a 24–78-mV lower reduction potential than a mutant with an alanine (Stephens et al., 1996). These are in good agreement with the observed decrease of 47 mV, although not as good when viewed in terms of the predicted relative ordering of the five mutants studied in this work. Moreover, the physical basis for the change was not elucidated because the two methods gave conflicting indications of the relative importance of protein dipoles, induced dipoles, and water. In fact, the somewhat polar SH group of a cysteine might be expected to increase the reduction potential relative to the methyl group of an alanine, instead of the observed decrease. Because their strategy is to calculate the difference in the total energy for a wild type and a mutant, it entails finding a small difference between many large contributions to the reduction potential.

The strategy used here is to correlate changes to due to individual residues with observed reduction potential differences in multiple homologous proteins. The first step is the calculation of the electrostatic potential contribution of individual residues from experimental structures of multiple homologous proteins. Residues are identified that show a correlation between the electrostatic contributions of specific amino acid types with known reduction potential differences. Because there are generally more sequences than structures of homologous proteins, the second step is examination of the amino acid types at the identified residue position in sequences of multiple homologous proteins. Likely sequence determinants of the reduction potential will show only a few different amino acid types in different homologous proteins and will be conserved in the more highly homologous proteins that have the same reduction

potentials. Moreover, if the electrostatic potential contribution of the identified residue and the reduction potential of the protein correlates with the amino acid type of the identified residue in many homologous proteins, then a site-specific mutation is likely to give the expected reduction potential shift because the effects of that residue appear independent of the local environment. This strategy will not identify reduction potential differences due to changes in solvent effects. In addition, for those sequence determinants that cause changes in the protein contribution to the electrostatic potential, this strategy will not identify additional changes in the electrostatic potential due to the solvent. However, this type of analysis of the Fe-S protein rubredoxin was used to identify an alanine versus a valine as the cause of an ~50-mV difference in reduction potentials via a 0.4-Å shift in the polar backbone, which alters the electrostatic environment of the [Fe] site (Swartz et al., 1996). Both the reduction potential shift and the backbone shift have now been confirmed experimentally by reduction potentials and crystal structures of site-directed mutants (Eidsness et al., 1999; Xiao et al., 2000).

Here, we examine the structure and energetics of the cysteines, both to characterize the putative SH···S hydrogen bonds in proteins as well as to assess the contributions of the cysteines to the redox site energetics of the ferredoxins. Specifically, we examine whether a cysteine at the Cys^x position can affect the reduction potential by altering the electrostatic environment and whether an SH···S hydrogen bond can stabilize a specific orientation of the cysteine so that it gives a consistent contribution to the electrostatic potential and thus the reduction potential. The focus is on cysteine relative to alanine in the Cys^x position; other residue types are discussed elsewhere (Q. Xie and T. Ichiye, unpublished results). First, the structures of cysteines and alanines relative to the redox site are examined in the 11 homologous ferredoxins with x-ray or NMR structures. A consistent structure for the cysteines indicates that the SH···S bond is stabilizing that conformation. In addition, consistent structures for all cysteines and for all alanines indicates that the conformation of each is relatively insensitive to the local environment and thus are likely to be adopted if mutations between alanines and cysteines are made. Second, the contributions of an alanine versus a cysteine at the Cys^x position to the electrostatic potential are determined using the experimental structures. These are used to elucidate how an alanine relative to a cysteine can cause the observed shifts in reduction potential. A discussion of these results follows.

METHODS

Structures and sequence alignments

The x-ray crystal and NMR solution structures and sequences for ferredoxins from 11 bacterial species (see Table 2) were obtained from the Protein Data Bank (PDB) (Bernstein et al., 1977), except for the re-sequenced and re-refined structure of Pa Fd (Backes et al., 1991), which was obtained from Elinor Adman at the University of Washington and is used rather than the older PDB entry (1FDX). For the 11 species, structures are available only for the protein in the fully oxidized state, except for the AvI Fd structure with a reduced [3Fe-4S] cluster. All crystal waters were retained. The Pf Fd sequence (Busse et al., 1992) was obtained from the Swiss Protein database (Genetics Computer Group, 1994).

Coordinates for polar hydrogens of the protein and water were generated using the molecular mechanics program CHARMM (24a3) (Brooks et al., 1983). The hydrogen coordinates were energy minimized with all other atoms fixed by exhaustive steepest-descents minimization until the gradient was less than 0.0001 kcal/mol (from less than 1,000 to over 10,000 steps). Partial charges appropriate to the oxidation states of the clusters were used with an atom-based force-switch on the non-bonded energy between 10 and 14 Å and a dielectric constant of 1.

A structure-based sequence alignment was performed for the 11 ferredoxins with known three-dimensional structures. First, pair-wise least-squares structural alignments were made of all equivalent atoms for each of the ligands to cluster 1 (see Table 3). For the two-cluster ferredoxins, an additional least-squares alignment was made of all equivalent atoms in both cluster 1 and cluster 2 redox site ligands. Residues with structurally homologous backbone conformations were then identified and used to create a structure-based sequence alignment. The sequence alignment for Pf ferredoxin was based on matching the redox site ligands.

Energy calculations

The contribution of protein residues to the energetics of the redox sites were evaluated via calculations of the electrostatic potentials and interaction energies. Similar calculations have been performed for the rubredoxins and HiPIPs except that the electrostatic potential at the redox site center was calculated (Swartz et al., 1996). The electrostatic energies may be related to redox properties using the relationship between the standard free energy change upon reduction, ΔG, and the reduction potential, $E°$, which is given by the Nernst equation:

$$-nFE° = \Delta G = \Delta E + \Delta PV - T\Delta S, \qquad (1)$$

where F is Faraday's constant, n is the number of electrons transferred, ΔE is the change in energy, ΔPV is the change in pressure and volume, T is the absolute temperature, and ΔS is the change in entropy. The change in electrostatic energy upon reduction, $\Delta E_e = E_e$(reduced) $- E_e$(oxidized), has been found to be the major contributing factor to ΔE (Shenoy and Ichiye, 1993). It has contributions of both the interaction energy between the redox site and the protein-plus-solvent environment surrounding the site and the interaction energy between atoms of the environment. This energy arises from changes in both the partial charges of the redox site and the coordinates of the entire system, the latter reflecting structural relaxation in response to the change in charge. However, if there is no structural relaxation (see Discussion), the interaction energy between atoms of the environment remains constant and the change is solely in the electrostatic interaction energy between the redox site and the environment. The contribution of a single residue, the Cys^x residue, to this interaction in one oxidation state is

$$E_x = \sum_i \sum_j \frac{q_i q_j}{r_{ij}}, \qquad (2)$$

where i is summed over the redox site atoms and j is summed over the Cys^x residue atoms, q_i is the charge of atom i, and r_{ij} is the distance between atoms i and j. Furthermore, the contribution to the change in electrostatic

TABLE 1 Redox site and cysteinyl atomic charges in units of electron charge

	Atom	Oxidized (−2)	Reduced (−3)
[4Fe-4S]*	Fe (A)	0.409	0.481
	Fe (B)	0.409	0.484
	S* (A)	−0.393	−0.523
	S* (B)	−0.393	−0.542
	Sγ (A)	−0.567	−0.724
	Sγ (B)	−0.567	−0.710
	Cβ (A)	0.051	0.014
	Cβ (B)	0.051	0.020
[3Fe-4S]*	Fe (A)	0.5469	0.6245
	Fe (B)	0.5469	0.6205
	S* (A)	−0.3914	−0.5628
	S* (B)	−0.3914	−0.5438
	Sγ (A)	−0.7544	−0.9675
	Sγ (B)	−0.7544	−0.9861
	Cβ (A)	0.0627	0.0914
	Cβ (B)	0.0627	0.0980
Cys		All-atom†	United atom
	CH_2	0.07	0.19
	S	−0.23	
	H	0.16	
	SH		−0.19

Based on Mouesca et al. (1994). See text. A atoms are bonded to non-delocalized Fe only, and B atoms are in delocalized Fe pair plane. See Fig. 3 for a schematic of this organization. Sγ is a sulfur from a cysteinyl ligand, and S is an inorganic sulfur.

†Cysteine side-chain atomic charges are based on CHARMM22 parameters. See text.

energy upon reduction of this residue with no structural relaxation is simply the negative of an electrostatic potential ϕ_x, which we define as

$$-nF\phi_x = \Delta E_x \text{ (no relaxation)} = \sum_i \sum_j \frac{\Delta q_i q_j}{r_{ij}}, \quad (3)$$

where Δq_i is the change in charge of redox site atom i upon reduction. Unless otherwise stated, ϕ_x was calculated using the crystal structure of the fully oxidized state with hydrogen coordinates generated with partial charges of the fully oxidized site with no cutoffs.

Energy parameters

Partial charges were taken from the CHARMM19 force field (Brooks et al., 1983), which has explicit polar hydrogens and implicit nonpolar hydrogens. However, because CHARMM19 uses a united-atom model for cysteinyl sulfhydryls, the explicit hydrogen cysteine side chain results used charges based on the all-atom CHARMM22 force field (MacKerell et al., 1998). In these modified parameters, the sulfur and the hydrogen have CHARMM22 charges, the methylene group has the net charge of the CHARMM22 charges for the carbon and explicit hydrogen (Table 1), the X-CH2E-S-X dihedral angle has parameters $k = 0.5$ kcal/mol and $n = 3$, and the rest of the parameters are CHARMM19 parameters. The united-atom cysteine side-chain results used CHARMM19 parameters (Table 1) exclusively.

Charges for the Fe-S redox site atoms (Table 1) were taken from density functional theory (DFT) quantum mechanical calculations of [4Fe-4S] analogs (Mouesca et al., 1994). Charges for [3Fe-4S] clusters were obtained from the [4Fe-4S] DFT charges by scaling Fe and cysteine ligand atom (but not S*) charges by 4/3, then adding a constant charge to every redox site atom such that the sum of the charges was appropriate for the oxidation state of the cluster. Both types of clusters have been shown to have valence delocalization over two or more of the Fe atoms (Holm, 1992), which is also observed in the DFT calculations of the [4Fe-4S] cluster (Mouesca et al., 1994). For the oxidized state, which is formally $Fe(II)_2Fe(III)_2$ for the [4Fe-4S] cluster and $Fe(III)_3$ for the [3Fe-4S] cluster, all of the irons are delocalized and thus equivalent. However, for the reduced state, which is formally $Fe(II)_3Fe(III)$ for the [4Fe-4S] cluster and $Fe(II)Fe(III)_2$ for the [3Fe-4S] cluster, here the Cys^1 and Cys^3 are bound to the valence delocalized Fe(II)Fe(III) pair (Fig. 3) based on ^{1}H-NMR results for *Thermococcus litoralis* Fd (Donaire et al., 1994).

RESULTS

The structural and energetic characteristics of the one- and two-cluster ferredoxins listed with abbreviations in Table 2 are presented in this section. Unless otherwise indicated, the highest resolution structures will be used and the residue numbering of AvI Fd will be used.

Sequence alignments

The sequences of 11 unique wild-type ferredoxins with x-ray or NMR structures were aligned (Table 3) via a structure-based sequence alignment procedure (see Methods). Cysteines 8, 11, 16, and 49 generally ligate cluster 1, which is present in all the ferredoxins, while cysteines 39, 42, 45, and 20 generally ligate cluster 2 in the two-cluster ferredoxins. Of the ferredoxins with [3Fe-4S] redox sites, all have the [3Fe-4S] site at cluster 1 and lack the Cys 11 ligand: Sa Fd has a C11D substitution whereas AvI and Bs Fd have an insertion at residues 12 and 13. Pf Fd has an unusual Asp 11 ligand. Only Cys 8, Cys 16, Pro 21, Cys 49, and Pro 50 are strictly conserved between one-cluster and two-cluster ferredoxins, so that the overall identity is only 11%. There are cysteines and predominantly alanines at the Cys^x position.

Structural comparisons

Of the five ferredoxins with extra cysteines that have experimental structures, Pa, Bs, and AvI Fd have the cysteine at residue 24 near cluster 2 and Cv and DaI Fd have it at residue 53 near cluster 1 (Fig. 1). Because residues 24 and 53 are four residues C-terminal to Cys^4 of cluster 2 and 1, respectively (Table 3), they are in structurally symmetric locations because of the quasi twofold rotational symmetry of the two-cluster ferredoxins about an axis normal to the β-sheet. If cluster 2 of Pa, Bs, and AvI Fd are structurally aligned with cluster 1 of Cv and DaI Fd in an inverse alignment, the extra cysteines in each ferredoxin are found to be almost structurally identical (Fig. 2). This inverse alignment for DaI with Pa and AvI Fd has been previously identified (Séry et al., 1994), but here the inverse alignment of Cv and Bs Fd are added. Moreover, the side-chain dihedral angles and distances from redox site sulfurs are quite similar for the extra cysteine in all five structures (Table 4).

TABLE 2 Bacterial ferredoxins with reported x-ray or NMR structures

Species*	Abbreviation	Cluster 1	Cluster 2	PDB code	Resolution (Å)
Peptostreptococcus asaccharolyticus	Pa	[4Fe-4S]	[4Fe-4S]	1FDX†	2.0
Chromatium vinosum	Cv	[4Fe-4S]	[4Fe-4S]	1BLU	2.1
Clostridium acidiurici	Ca	[4Fe-4S]	[4Fe-4S]	2FDN	0.94
				1FDN	1.84
Clostridium pasteurianum	Cp	[4Fe-4S]	[4Fe-4S]	1CLF	NMR
Azotobacter vinelandii	AvI	[3Fe-4S]	[4Fe-4S]	7FD1	1.30
				6FD1	1.35
				5FD1	1.9
Azotobacter vinelandii‡	AvI′	[3Fe-4S]	[4Fe-4S]	2FD2	1.9
Bacillus schlegeli	Bs	[3Fe-4S]	[4Fe-4S]	1BD6	NMR
Bacillus schlegeli§	Bs′	[4Fe-4S]	[4Fe-4S]	1BQX	NMR
Sulfolobus acidocaldarius	Sa	[3Fe-4S]	[3Fe-4S]	1XER	2.0
Desulfovibrio africanus	DaI	[4Fe-4S]	None	1FXR	2.3
Bacillus thermoproteolyticus	Bt	[4Fe-4S]	None	2FXB	2.3
Thermotoga maritima	Tm	[4Fe-4S]	None	1VJW	1.75
Desulfovibrio gigas	DgII	[3Fe-4S]	None	1FXD	1.7
Pyrococcus furiosus	Pf	[4Fe-4S]	None	NA	NA

*Pa (Backes et al., 1991), Cv (Moulis et al., 1996), Ca (Dauter et al., 1997; Duée et al., 1994), Cp (Bertini et al., 1995), AvI (Stout et al., 1998; Stout, 1993; Schipke et al., 1999), AvI′ (Soman et al., 1991), Bs and Bs′ (Aono et al., 1998), Sa (Fujii et al., 1996), DaI (Séry et al., 1994), Bt (Fukuyama et al., 1989), Tm (Sticht et al., 1996), DgII (Kissinger et al., 1991).

†A revised structure was obtained directly from Elinor Adman at the University of Washington. This structure has not yet been released to PDB.

‡Structure of a mutant, C24A.

§Structure of a mutant, D11C (AvI numbering) or D13C (Bs numbering).

From the hydrogen coordinate generation, three energy minima for the cysteinyl Cα-Cβ-Sγ-Hγ dihedral angle are found near $-60°$, $+60°$, and $+180°$ (Fig. 3; Table 4). Here, the Sγ distances to the redox sulfurs (Table 4) are all fixed for all three orientations (the crystal coordinates are used for all non-hydrogen atom positions), and the only difference between the three orientations is the hydrogen position. Even though Cys Sγ···S*[2] is the shortest sulfur-to-sulfur distance, no linear hydrogen bonds can be formed to it in any of the orientations unless the heavy atoms of the side chain are moved from their crystal coordinate positions. In the $-60°$ orientation, the Cys Sγ hydrogen bonds to the redox site Sγ^4. In AvI Fd, the Cys Sγ···Sγ^4 and Cys Hγ···Sγ^4 distances are 3.64 and 2.43 Å, respectively, while the

TABLE 3 Sequence alignment of bacterial ferredoxins based on backbone structural alignment

Ferredoxin	Amino acid sequence*							$E°$ (mV)	
	0	10	20	30	40	50		#1	#2
Two cluster									
Ca	...AYVINEACIS	CG..ACEPEC	PVN**A**ISSGDD..	RYVID..ADTCI	DCG.ACAGVCP	VD**A**PVQA		−420	−420
Cp	...AYKIADSCVS	CG..ACASEC	PVN**A**ISQGDS..	IFVID..ADTCI	DCG.NCANVCP	VG**A**PVQE		−390	−390
Pa	...AYVINDSCIA	CG..ACKPEC	PVN**C**IQEG.A..	IYAID..ADSCI	DCG.SCASVCP	VG**A**PNPED		−427	−427
Cv	...ALMITDECIN	CD..VCEPEC	PNG**A**ISQGDE..	TYVIE..PSLCT	ECVaQCVEVCP	VD**C**IIKDP21Δ		−482	−482
AvI†	...AFVVTDNCIK	CKYTDCVEVC	PVD**C**FYEGPN..	FLVIH..PDECI	DCA.LCEPECP	AQ**A**IFSED48Δ		−425	−647
Bs§	...AYVITEPCIG	TKDASCVEVC	PVD**C**IHEGED..	QYYID..PDVCI	DCG.ACEAVCP	VS**A**IYHED19Δ		N/A	N/A
Sa	36ΔVGVDFDLCIA	DG..SCINAC	PVN**V**FQWYDTPb	KKADPVNEQACI	FCM.ACVNVCP	VA**A**IDVKPP		N/A	N/A
		•	• • €	↑	€	€ € •	↑		
One cluster									
Bt	PKYTIVDKETCIA	CG..ACGAAA	P.D**I**YDYDEDG.	IAYVTLDcDILI	DDMMDAFEGCP	TD**S**IKVAD11Δ		−280	
Pf	AWKVSVDQDTCIG	DA..ICASLC	P.D**V**FEMNDEG.	KAQPKVEdEELY	NCAKEAMEACP	VS**A**ITIEEA		−375	
Tm	.MKVRVDADACIG	CG..VCENLC	P.D**V**FQLGDDG.	KAKVLQPETDL.	PCAKDAADSCP	TG**A**ISVEE		N/A	
DgII	..PIEVNDD.CMA	CE..ACVEIC	P.D**V**FEMNEEGD	KAVVINPDSDL.	DCVEEAIDSCP	AE**A**IVS-		130(−450)§	
DaI	ARKFYVDQDECIA	CE..SCVEIA	P.G**A**FAMDPEIE	KAYVKDVEGASQ	EEVEEAMDTCP	VQ**C**IHWEDE		−385	
		• • •			•	↑			

*The numbering for AvI is used throughout. Symbols are defined as follows: •, cysteine ligands for cluster 1; €, cysteine ligands for cluster 2; ↑, extra cysteine; *n*Δ, *n* additional N- or C-terminal residues; a = GHYETS, b = GHPASE, c = DNQGIVEVP, and d = VIED.

†Sequence for mutant differs by C24A.

‡Sequence for 2[4Fe-4S] mutant differs by D11C (AvI numbering) or D13C (Bs numbering).

§DgII Fd has a [3Fe-4S] cluster that can be converted to a [4Fe-4S] cluster; reduction potentials are for [3Fe-4S] ([4Fe-4S]).

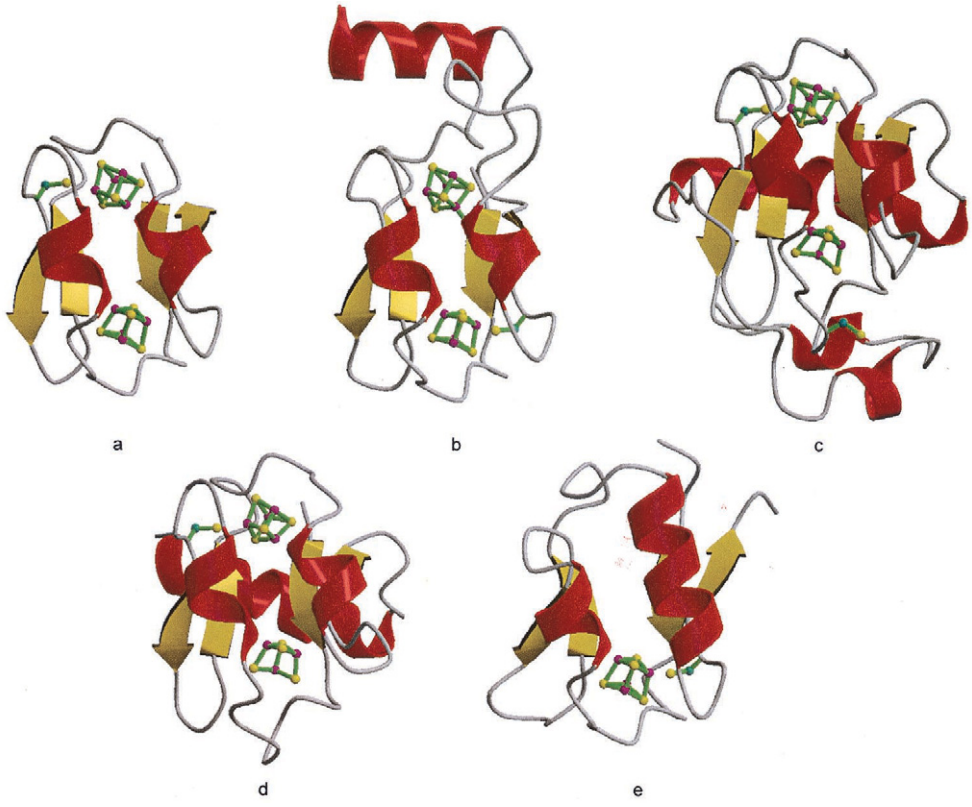

FIGURE 1 Structure of ferredoxins from Pa (*a*), Cv (*b*), AvI (*c*), Bs (*d*), and DaI (*e*). The secondary structural elements are α-helices (*red*), β-sheets (*yellow*), and coil (*white*). The redox cluster, the extra cysteine, and another cysteine in AvI, which is its potential third ligand, are shown in ball-and-stick representation with sulfurs (*yellow*), irons (*magenta*), and carbons (*cyan*) as balls. In each case, cluster 1 is the lower cluster and cluster 2 is the upper cluster. This figure was generated using MOLSCRIPT (Kraulis, 1991) and Raster3D (Merritt and Murphy, 1994).

Cys$S\gamma\cdots S^{*2}$ and Cys$H\gamma\cdots S^{*2}$ distances are 3.36 and 3.58 Å, respectively, and the Cys$S\gamma\cdots S^{*3}$ and Cys$H\gamma\cdots S^{*3}$ distances are 3.89 and 3.60 Å, respectively. Because the $S\gamma$—$H\gamma$ bond length is 1.325 Å, a linear hydrogen bond is formed to $S\gamma^4$ whereas only perpendicular hydrogen bonds can be made to S^{*2} and S^{*3}. Furthermore, in the +60° and 180° orientations, no linear hydrogen bonds can be made to any of the sulfurs (Fig. 3). The best electrostatic interaction energy between the cysteine side chain and the nearest cluster E_x (see Methods) in the oxidized state is for the −60° orientation because of the hydrogen bond to $S\gamma^4$ (Table 5); thus, it is used for all further calculations. Moreover, the E_x using the united-atom approximation (see Methods) for the SH group of the extra cysteine are significantly higher than any of the explicit hydrogen (see Methods) results.

The NMR structure of Bs′ Fd, the D11C (AvI numbering) mutant of Bs Fd, demonstrates the effects of [3Fe-4S] to [4Fe-4S] cluster conversion. Although the conversion is of cluster 1, it also affects the extra cysteine near cluster 2 because this cysteine is close in sequence to the first three ligands of cluster 1. In the wild type, the Cys$S\gamma$ is further from the [3Fe-4S] cluster than in the other ferredoxins whereas, in the mutant, it approaches closer to the [4Fe-4S] cluster at a distance much more like the other ferredoxins (Table 4).

Electrostatic potential calculations

The contributions to the electrostatic potential of the Cys^x position, ϕ_x (see Methods), of a cysteine as well as the amide N to the $S\gamma^4$ of the redox site distance ($N\cdots S\gamma^4$) were also examined (Table 6). In addition, the average and standard deviation of these values in the wild-type structures are reported for cysteines and for alanines at this position. The individual values for each alanine are reported and examined elsewhere (Q. Xie and T. Ichiye, unpublished results). The side chain of the extra cysteine actually raises ϕ_x of the nearest cluster by ~8 mV in all five cases using the modified CHARMM22 parameters for the side chain (Table 1), but this amount is essentially insignificant. However, the backbone contribution of the cysteine is ~130 mV whereas the contribution of the alanine in the equivalent position is ~200 mV. This is because the backbone is slightly further from the redox site for cysteines than for alanines (the $N\cdots S\gamma^4$ distances are ~3.6 and 3.4 Å, respectively). Thus, the extra cysteine lowers ϕ_x of the nearest cluster by ~60 mV in all five cases, but the

FIGURE 2 Inverse alignment of cluster 1 from Cv (*purple*) and DaI (*white*) with cluster 2 from Pa (*dark blue*), AvI (*red*), and Bs (*light blue*). The protein backbones and the extra cysteines are shown as licorice models (white side chain is completely within the other four) while the cluster is represented as in Fig. 1. This figure was generated using MOLSCRIPT (Kraulis, 1991) and Raster3D (Merritt and Murphy, 1994).

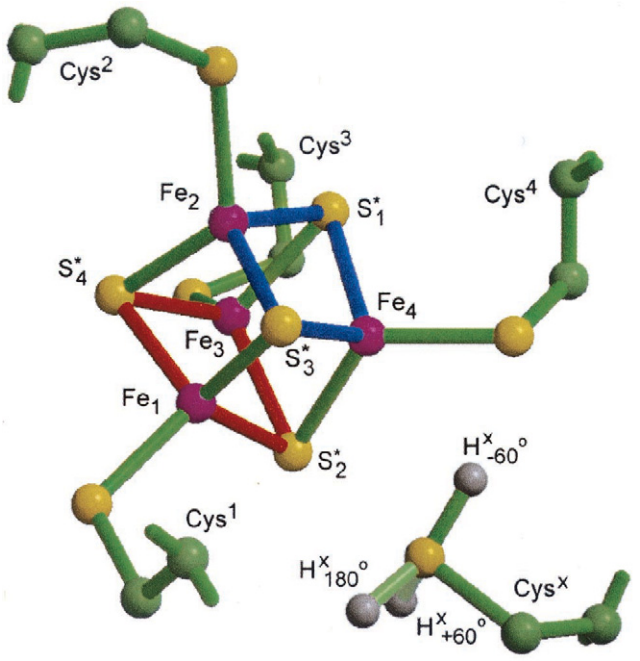

FIGURE 3 [4Fe-4S] redox site geometry of cluster 2 along with the extra cysteine in AvI Fd. The atoms are sulfur (*yellow*), iron (*magenta*), carbon (*cyan*), and hydrogen (*white*). The plane of the cluster containing the non-delocalized pairs is indicated by blue bonds and the delocalized pairs by red bonds. The three conformations of the hydrogen are indicated as +60°, −60°, and 180°, which correspond to approximate values of Cα-Cβ-Sγ-Hγ, with the SH bonds of the less favored +60° and 180° conformations shaded lighter. This figure was generated using MOLSCRIPT (Kraulis, 1991) and Raster3D (Merritt and Murphy, 1994).

change is mainly due to the backbone. The united-atom approximation using the CHARMM19 parameters for the side chain (Table 1) gives a side-chain contribution to ϕ_x of ~−110 mV, which is much different from the explicit hydrogen value of +8 mV. The values for both alanines of AvI′ Fd, which is the mutant of AvI that has a Cys→Ala mutation at the Cys^x position near cluster 2, and for the alanine of the wild-type AvI are also reported (Table 6). Interestingly, in AvI′ Fd, the contribution to ϕ_x and $N \cdots S\gamma^4$ distance of the mutant alanine is closer to that of the cysteine average than the alanine average.

The effects of the resolution of the structure on ϕ_x are also examined because the accuracy of the structure will play a role in the accuracy of the energetics. The results for AvI Fd at 1.35-Å (6FD1) vs. 1.9-Å (5FD1) resolution and Ca Fd at 0.94-Å (2FDN) vs. 1.84-Å (1FDN) resolution (Table 7) indicate very little effect.

Finally, the effects of structural relaxation (see Methods) are examined, where structural relaxation refers to the changes in the three-dimensional structure of the protein

TABLE 4 Geometry of the cysteine at the Cys^x position: dihedral angles and interatomic distances to nearest cluster

Protein	Cluster	N-Cα-Cβ-Sγ (°)	Cα-Cβ-Sγ-Hγ			Sγ···S*[2] (Å)*	Sγ···Sγ[4] (Å)*
			Near −60° (°)	Near +60° (°)	Near 180° (°)		
Pa	2	64	−57	69	156	3.63	3.68
Cv	1	73	−50	61	152	3.62	3.73
AvI	2	58 ± 4	−53 ± 1	60 ± 0	154 ± 1	3.36 ± 0.01	3.62 ± 0.02
Bs	2	71	−62	70	147	3.89	4.04
DaI	1	57	−55	58	172	3.35	3.57
AVE†		65 ± 7	−55 ± 4	64 ± 6	156 ± 9	3.57 ± 0.21	3.73 ± 0.17
Bs′‡	2	73	−58	61		3.54	3.59

*The first atom from the Cys^x residue and the second atom from the nearest cluster.
†Average of five wild-type structures.
‡2[4Fe-4S], D13C mutant.

TABLE 5 Cysteine side-chain E_x in the oxidized state for the united-atom approximation and for different conformations of Cα-Cβ-Sγ-Hγ dihedral

Protein	Cluster	United atom (kcal/mol)	Near −60° (kcal/mol)	Near +60° (kcal/mol)	Near 180° (kcal/mol)
Pa	2	4.6	−1.2	1.9	3.2
Cv	1	4.3	−1.7	2.2	3.2
AvI	2	4.8 ± 0.1	−1.0 ± 0.1	2.0 ± 0.1	2.8 ± 0.1
Bs	2	4.2	−1.7	2.9	3.4
DaI	1	5.0	−0.8	1.6	3.2
AVE*		4.6 ± 0.3	−1.3 ± 0.4	2.1 ± 0.5	3.1 ± 0.3
Bs′†	2	4.9	−1.9	2.8	

*Average of five wild-type structures.
†2[4Fe-4S], D13C mutant.

TABLE 7 Cys^x residue distance to the nearest cluster and contribution to ϕ_x of the nearest cluster: effects of resolution of structure

Protein	Cluster	Cys^x residue	Resolution (Å)	N···Sγ^4 (Å)	ϕ_x* BB (mV)	ϕ_x* PSC (mV)	ϕ_x* BB+PSC (mV)
Ca	1	Ala	0.94	3.33	230	0	230
Ca	1	Ala	1.84	3.26	231	0	231
Ca	2	Ala	0.94	3.31	172	0	172
Ca	2	Ala	1.84	3.16	208	0	208
AvI	1	Ala	1.30	3.39	207	0	207
AvI	1	Ala	1.35	3.40	209	0	209
AvI	1	Ala	1.9	3.31	217	0	217
AvI	2	Cys	1.30	3.58	117	−7	110
AvI	2	Cys	1.35	3.61	122	−3	119
AvI	2	Cys	1.9	3.62	113	−9	105

*BB, backbone amides and carbonyl; PSC, polar side chains with no net charge.

upon change in oxidation state of the redox site. Because AvI Fd is the only case with experimental structures of reduced protein, the effects are calculated for AvI Fd at pH 8 using the oxidized (6FD1 at 1.35-Å and 7FD1 at 1.30-Å resolution) and reduced (6FDR at 1.40-Å and 7FDR at 1.40-Å resolution) structures (Schipke et al., 1999) (Table 8). The oxidized state is $Fe_3S_4(SR)_3^{2-}$-$Fe_4S_4(SR)_4^{2-}$ whereas the reduced structure is reduced only in the [3Fe-4S] cluster 1 so that the reduced state is $Fe_3S_4(SR)_3^{3-}$-$Fe_4S_4(SR)_4^{2-}$; hence, for this part, reduced refers to reduction only at cluster 1. In all of the values of ΔE_x (the difference in E_x between the oxidized and reduced states; see Methods), the oxidized state is the same. In the relaxed results for ΔE_x (ro,ro,ro in Table 8), E_x for the reduced state uses reduced partial charges and the reduced structure with hydrogen coordinates generated with reduced partial charges. For comparison, in the unrelaxed results for ΔE_x (oo,oo,or in Table 8), E_x for the reduced state uses the oxidized structure with hydrogens generated using oxidized charges, so that $\Delta E_x = -nF\phi_x$. Also, in the relaxed hydrogen results for ΔE_x (oo,ro,ro in Table 8), E_x for the reduced state uses the oxidized structure with hydrogens generated using the reduced charges so that the effects of hydrogen coordinate generation can be examined. At both pH states and at either cluster, the energetics of the cysteine or alanine at the Cys^x position are minimally affected by relaxation.

DISCUSSION

The observation of close interactions of extra cysteines with sulfurs that do not ligate redox site metals with redox site sulfurs in five homologous ferredoxins indicates the formation of a SH···S hydrogen bond, which has significant implications for the electron transfer energetics of these proteins. The results here are based on comparisons of the electrostatics from multiple homologous protein experimen-

TABLE 6 Cys^x residue distance to the nearest cluster and contributions to ϕ_x of the nearest cluster

Cys^x residue	Protein	Cluster	N···Sγ^4 (Å)	ϕ_x* NPSC (mV)	ϕ_x* BB (mV)	ϕ_x* PSC (mV)	ϕ_x* BB+PSC (mV)
Cys	Pa	2	3.44	−112	139	6	145
	Cv	1	3.79	−110	109	16	125
	AvI	2	3.60 ± 0.02	−120 ± 1	120 ± 4	−5 ± 3	114 ± 6
	Bs	2	3.68	−99	114	25	139
	DaI	1	3.63	−120	178	−3	175
	AVE†		3.63 ± 0.12	−112 ± 8	132 ± 27	8 ± 12	140 ± 21
	Bs′‡	2	3.71	−115	87	19	106
Ala	AVE§		3.38 ± 0.07	0	202 ± 40	0	202 ± 40
	AvI	1	3.40 ± 0.01	0	208 ± 1	0	208 ± 1
	AvI′¶	1	3.32	0	229	0	229
	AvI′¶	2	3.54	0	141	0	141

*BB, backbone amides and carbonyl; PSC, polar side chain with no net charge; NPSC, polar side chain using the united-atom approximation for the cysteinyl SH group.
†Average of all cysteines in the five wild-type structures with cysteines.
‡2[4Fe-4S], D13C mutant.
§Average of all alanines in the nine wild-type structures with alanines.
¶C24A mutant.

TABLE 8 Cys^x residue distance to the nearest cluster and contribution to ΔE_x of the nearest cluster: effects of relaxation in AvI Fd

Cluster	Cys^x residue	Reduced conditions	N···Sγ^4 (Å)	$-\Delta E_x/nF$* BB (mV)	PSC (mV)	BB+PSC (mV)
1	Ala	oo,oo,ro	3.39 ± 0.01	208 ± 1	0	208 ± 1
1	Ala	oo,ro,ro	3.39 ± 0.01	210 ± 1	0	210 ± 1
1	Ala	ro,ro,ro	3.42 ± 0.06	221 ± 26	0	221 ± 26
2	Cys	oo,oo,ro	3.60 ± 0.02	0	0	0
2	Cys	oo,ro,ro	3.60 ± 0.02	0 ± 0	1 ± 1	1 ± 0
2	Cys	ro,ro,ro	3.60 ± 0.08	18 ± 15	0 ± 2	18 ± 15

*BB, backbone amides and carbonyl; PSC, polar side chains with no net charge. ΔE_x is calculated with the following conditions: oo,oo,oo for the oxidized state and the above list for the reduced state. The conditions are described by two letters describing the state of cluster 1 and cluster 2 as either oxidized (o) or reduced (r). The first set of conditions refers to the structure used (Schipke et al, 1999): 00 = 6FD1 and MFD1 and ro = 6FDR and 7FDR. The second set refers to the partial charges during hydrogen coordinate generation, and the third set refers to partial charges used during ΔE_x calculation.

tal structures and of amino acid types in multiple homologous protein sequences, which comprise our approach as described in the Introduction. The accuracy of the experimental structures has relatively little effect at the resolutions of the structures here, as shown by comparisons of structures at different resolutions (Table 7). The key is finding results that are consistent in structures of multiple homologous proteins.

Structure and energetics

The 11 homologous ferredoxins have cysteines or alanines at the Cys^x position. Alignment shows the remarkable structural similarity of the cysteines and of the alanines. The contributions to the electrostatic potential of cysteines at the Cys^x position ϕ_x are also quite similar for the homologous proteins, as are those of alanines. This implies that the structure and energetics of the residue at the Cys^x position is dependent only on its amino acid type and not the local protein environment even though the proteins have very different sequences (Table 3). Thus, both residues 24 and 53 are prime candidates for site-directed mutations of Ala↔Cys.

Hydrogen bonds

The negative interaction energy of the extra cysteine with the redox site in the oxidized state (Table 5) indicates a SH···S hydrogen bond; i.e., E_x of the −60° conformation is −1 to −2 kcal/mol, in agreement with quantum calculations (Koerner and Ichiye, 2000; Beck, 1997). Moreover, E_x is much more favorable when the SH···S hydrogen bond is included than when a united-atom approximation is used; i.e., E_x of the −60° conformation is ~6 kcal/mol lower than that of the united-atom approximation. The SH···S hydrogen bond is apparently important in stabilizing the side-chain conformation of the cysteine found in all of the experimental structures (Table 4). Moreover, in molecular dynamics simulations of Pa and AvI Fd using the united-atom approximation for the cysteinyl SH group, the cysteine in the oxidized state moves away from the cubane (Sγ moves ~0.5 Å) and in the reduced state actually moves into solution (Sγ moves ~6 Å), due to the electrostatic repulsion between the negative partial charges of the SH group and the redox site (Beck, 1997). In more recent molecular dynamics simulations of Pa Fd using explicit hydrogens for the cysteinyl SH group with the same partial charges as used here, the cysteine maintains the conformation seen in experimental structures (Beck, 1997; E. A. Dolan and T. Ichiye, unpublished results).

Implications for reduction potentials

Although examining the contributions of individual residues to the electrostatic potential does not allow comparison with absolute reduction potentials, the differences in contributions to the electrostatic potential of cysteines versus alanines at the Cys^x position can be a good indicator of differences in reduction potential due to the identity of the amino acid at that position. If there are no insertions and deletions as in the case of the rubredoxin study (Swartz et al., 1996), differences in reduction potential between homologous proteins can be predicted. However, here most of the ferredoxin sequences have insertions and deletions (Table 3) so that there are likely to be other contributing factors, such as differences in solvation, and the 2[4Fe-4S] ferredoxins are complicated by the two clusters. Fortunately, there are mutational data in which the C24A mutation in AvI ferredoxin increases the reduction potential by 47 mV (Iismaa et al., 1991) and the A53C (A60C in Pf numbering) mutation in Pf ferredoxin decreases the reduction potential by 37 mV (Brereton et al., 1998), so that a cysteine at the Cys^x position changes the reduction potential by ~−50 mV relative to an alanine.

Our results indicate the total change in ϕ_x of the nearest cluster for Ala→Cys at the Cys^x position is ~−60 mV (Cys AVE versus Ala AVE BB+PSC in Table 6), which is in good agreement with the experimental results for the reduc-

tion potential. The cysteine side chain using charges based on CHARMM22 parameters (Table 1) contributes ~10 mV to the ϕ_x (Cys AVE PSC in Table 6), which is a very small shift in the opposite direction of the reduction potential shift and is due to the polar SH group. However, the backbone contribution to ϕ_x of a cysteine at the Cys^x position is ~70 mV lower than that of an alanine (Cys AVE versus Ala AVE BB in Table 6) due to the backbone of the alanine approaching closer to the redox site (Table 6) because of its smaller side chain. In addition, ϕ_x calculated with a united-atom approximation for the SH group using CHARMM19 parameters (Table 1) is very negative compared with the explicit hydrogen result (NPSC versus PSC in Table 6) so that the agreement with the experimental reduction potential shifts is worse. These values are calculated using CHARMM19 parameters, which is still a widely used force field. The results would change only qualitatively with all-atom CHARMM22 parameters because the major difference between the parameters for the interactions studied here is the increased polarity of the NH group, which would serve to increase the difference due to the backbone shift. Thus, including the SH···S interaction is necessary for obtaining the correct ϕ_x. Moreover, the SH···S bond stabilizes the correct backbone conformation.

An important factor here is that the Cys^x residue adopts the same conformation in multiple experimental structures. Even though some of the cysteines are located near cluster 1 and some are located near cluster 2 in the available experimental structures, these are quasi-equivalent environments (Fig. 2), and so there are five different cases where the cysteine adopts the same side-chain conformation and backbone position. Similarly, there are 11 different cases where the alanine adopts the same backbone position. The multiplicity of structures indicates that the backbone shift between the cysteine and the alanine is significant because the actual shift is quite small. In addition, the different experimental structures are of different homologous proteins, which have the same basic backbone structure around each redox site (Fig. 2) but differ considerably in the surrounding side chains. The multiplicity of side-chain environments indicates that the cysteine side-chain conformation is stable and that mutations in a variety of different ferredoxins between cysteine and alanine are likely to give the same backbone shifts and thus reduction potential shifts.

There are also other possible contributing factors to the changes in reduction potential upon mutation (Swartz et al., 1996; Stephens et al., 1996; Ichiye, 1999). Our approach will not identify changes due to solvent accessibility such as occur with insertions and deletions and is more reliable in identifying changes due to buried nonpolar or polar residues, which may be considered to be uncoupled from the solvent so that their contributions to the reduction potential are additive electrostatic contributions. Because the Cys^x residue is relatively buried, changes in the solvation are unlikely. The possibility of water entering a pocket created by the smaller alanine relative to the cysteine was examined, but no waters were found in any of the structures. Entropic effects (see Methods) are also likely to be small because the change in entropy upon reduction should be small regardless of the amino acid type. The effects of structural relaxation are also ignored because, unfortunately, there is only one ferredoxin that has structures for both oxidation states. For the one case where there is a reduced structure, AvI Fd, the comparison of the relaxed and unrelaxed results indicates that relaxation makes a small contribution (~10–20 mV) to the energetics of the Cys^x position (Table 8). However, the polar side chain of the cysteine would be more affected than the more restrained backbone of either the cysteine or the alanine, and the cysteine is located near the [4Fe-4S] site whereas the reduction was at the [3Fe-4S] site. The most likely contributing factor is other shifts in the local environment; in particular, the backbone shift may be propagated to neighboring residues. On average, the Cys^x−1 residue backbone contributes another −10 mV (166 ± 8 for Ala vs. 156 ± 19 for Cys) and the Cys^x+1 residue contributes another −20 mV (40 ± 28 for Ala vs. 20 ± 12 for Cys) to the electrostatic potential so that the total change is ~−90 mV.

Mutant structures

The crystal structure of AvI′ Fd, the C24A mutant of AvI Fd, allows direct evaluation of the effects of an Ala↔Cys mutation on ϕ_x. Interestingly, the backbone of the alanine does not shift inward as much (Table 6), and ϕ_x is much smaller than that for most of the alanines at the Cys^x position so that the total change in ϕ_x between Ala→Cys is −22 mV (Cys AvI′ cluster 2 versus Cys AvI cluster 2 BB+PSC in Table 6), which is in remarkably good agreement with the measured reduction potential shift of −47 mV. Moreover, it is somewhat smaller than the shift predicted from the average of all the alanines and all of the cysteines at the Cys^x position (Ala AVE versus Cys AVE BB+PSC in Table 6). Again, other changes in the local environment are probably responsible for further shifts in the electrostatic potential. For instance, examination of the backbone electrostatic contributions of the neighboring residues indicates that the Cys^x−1 contributes −14 mV and Cys^x+1 contributes 9 mV, for a total change for Ala→Cys due to Cys^x−1, Cys^x, and Cys^x+1 of −27 mV, which is in slightly better agreement with the predicted shift.

The structure of AvI′ Fd also allows investigation of why the alanine in the C24A mutant has a smaller contribution than the alanines at the Cys^x position in the other homologous proteins (i.e., in Table 6, why Cys AvI′ cluster 2 BB+PSC is smaller than Ala AVE BB+PSC). For comparison, Cv Fd was chosen over Pa Fd because it has an isoleucine (the consensus residue type) at the Cys^x+1 position at both clusters whereas Pa Fd has a less common proline. The structure of Cv Fd at the Cys^x positions near

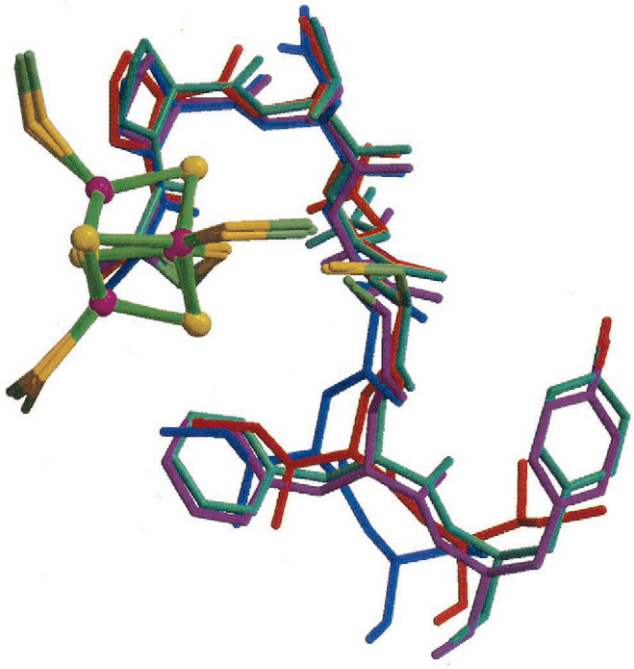

FIGURE 4 Comparison of the Cys^x region for the wild-type and mutant AvI Fd with the wild-type Cv Fd: the wild-type AvI Fd cluster 2 region with a cysteine (*light blue*), the mutant AvI Fd cluster 2 region with the mutated alanine (*purple*), the Cv Fd cluster 1 region with a cysteine (*orange*), and the Cv Fd cluster 2 region with an alanine (*dark blue*). The Cys^x side-chain carbons (*light green*) and sulfurs (*yellow*) and the AvI Fd tyrosine oxygen (*red*) are also indicated. This figure was generated using MOLSCRIPT (Kraulis, 1991) and Raster3D (Merritt and Murphy, 1994).

both clusters illustrates how the smaller side chain of the alanine relative to the cysteine allows the backbone to shift closer to its cluster (Fig. 4). The backbone of the wild-type cysteine in AvI Fd is very similar to that of the cysteine in Cv Fd whereas the backbone of the mutated alanine in AvI′ Fd is very different from that of the alanine in Cv Fd and is much closer to that of the cysteine in AvI Fd and Cv Fd (Fig. 4). Most likely, the alanine of AvI′ Fd cannot shift closer to the redox site because of neighboring residues. First, the Cys^x+1 residue is a phenylalanine, which is much bigger than the consensus isoleucine found in Cv Fd and may sterically hinder the shift. The only other phenylalanine at the Cys^x+1 position is in Sa Fd, which exhibits the larger distance from the redox site ($N\cdots S\gamma^4$ is 3.78 Å) seen for the alanine in AvI′ Fd and for cysteines in general. However, Sa Fd has a valine at the Cys^x position so it is not clear whether the larger distance is due to the valine or the phenylalanine. Second, the Cys^x+2 residue is a tyrosine, which is larger than most of the other amino acid types found here and is solvated at the surface. However, there is also a tyrosine at the Cys^x+2 position and an alanine at the Cys^x position in Bs Fd, which has the backbone shifted inwards ($N\cdots S\gamma^4$ is 3.24 Å) like the alanines in general. Thus, it would be of interest to see whether the additional mutations F25I and/or Y26S in AvI′ Fd cause the reduction potential to increase even more relative to wild type by allowing the alanine to move closer to the redox site. In addition, it would be of interest to see whether the reverse mutations in a ferredoxin with an alanine at the Cys^x position cause the reduction potential to decrease. The smaller change in reduction potential between the wild type and the Ala→Cys mutant of Pf Fd suggests that the alanine may also be in the same relative position as in AvI′ Fd, although it may also be due to the unusual aspartic acid ligand; unfortunately, no structural information is available.

CONCLUSIONS

X-ray crystal or NMR solution structures for five bacterial [4Fe-4S]-type ferredoxins indicate the presence of a putative SH···S hydrogen bond between redox site sulfurs and a nearby cysteine residue that does not ligate the redox site. The extra cysteine is located at either of the quasi twofold rotationally related locations four residues C-terminal to the fourth cysteinyl ligand of either cluster and always has the same side-chain conformation. The other residue types occurring at the extra cysteine position in the 11 homologous ferredoxins with experimental structures were mainly alanines. The SH···S hydrogen bond between the cysteinyl sulfur and a redox site sulfur was found to stabilize the side-chain conformation found in all five experimental structures of ferredoxins with the extra cysteine; i.e., the interaction of the cysteine with the redox site sulfurs is attractive so that its contribution to the electrostatic potential is positive. However, in the conformation stabilized by the SH···S hydrogen bond, the cysteine pushes the backbone further from the redox site than an alanine, which decreases the electrostatic potential. Thus, the net effect of the extra cysteine is that it decreases the calculated electrostatic potential by ~60 mV, in agreement with the C24A mutation in *A. vinelandii* ferredoxin (Iismaa et al., 1991) and the A53C (*A. vinelandii* numbering, A60C in *P. furiosus* numbering) mutation in *P. furiosus* ferredoxin (Brereton et al., 1998) in which a cysteine at this position decreases the experimental reduction potential by ~40–50 mV relative to an alanine. Other work indicates that a serine actually shifts the electrostatic potential upwards rather than downwards with respect to an alanine because it adopts a different side-chain conformation than a cysteine (Q. Xie and T. Ichiye, unpublished results). Natural instances of serine appear rare, possibly because nature has not found a use for a ferredoxin with a higher reduction potential (M.J. Fajardo and T. Ichiye, unpublished results).

In summary, an extra cysteine can tune the reduction potential of a ferredoxin by changing the electrostatic potential. For the residue position here, the SH···S hydrogen bond plays an important role by stabilizing the conformation of the extra cysteine, and although the backbone position plays the most important role in the electrostatic po-

tential with little direct contribution from the SH group, the conformation of the cysteine is important in determining the backbone position. The multiple structures showing consistent results for all cases with cysteines and for all cases with alanines indicate that the backbone shift is real and that mutations between cysteines and alanines will produce this shift in a variety of local side-chain environments. These results indicate that the extra cysteine may play an important role in the structure/function of the ferredoxins and, more generally, that hydrogen bonds involving sulfur can play an important role in protein structure and function. In addition, these results indicate that sequence differences that cause shifts of the polar backbone can alter the electrostatic environment of a redox site, thus changing the redox properties of a protein and, by inference, the electrostatic environment of an enzyme active site, thus changing the enzymatic activity of a protein.

We thank Dr. Michael W. W. Adams for providing reduction potentials for the mutant *P. furiosus* ferredoxin before their publication and Dr. Elinor Adman for providing the *P. asaccharolyticus* ferredoxin coordinates and sequences before their publication.

This work was supported by a grant from the National Institutes of Health (GM45303). Computation was performed on a 16-processor, high-performance parallel IBM SP (9076) funded by the National Science Foundation (BIR-9512538) and Washington State University. Additional computer time was provided by the Maui High Performance Computing Center (sponsored in part by the Phillips Laboratory, Air Force Materiel Command, USAF, under cooperative agreement number F29601–93-2–0001). The views and conclusions contained in this document are those of the authors and should not be interpreted as necessarily representing the official policies or endorsements, either expressed or implied, of Phillips Laboratory or the U.S. Government. We also thank the VADMS Laboratory at WSU for additional computational resources.

REFERENCES

Adman, E. T., L. C. Sieker, and L. H. Jensen. 1973. The structure of a bacterial ferredoxin. *J. Biol. Chem.* 248:3987–3996.

Adman, E. T., K. D. Watenpaugh, and L. H. Jensen. 1975. NH···S hydrogen bonds in *Peptococcus aerogenes* ferredoxin, *Clostridium pasteurianum* rubredoxin and *Chromatium* high potential iron protein. *Proc. Natl. Acad. Sci. U.S.A.* 72:4854–4858.

Aono, S., D. Bentrop, I. Bertini, A. Donaire, C. Luchinat, Y. Kiikura, and A. Rosato. 1998. Solution structure of the oxidized Fe_7S_8 ferredoxin from the thermophilic bacterium *Bacillus schlegelii* by ^{1}H NMR spectroscopy. *Biochemistry.* 37:9812–9826.

Backes, G., Y. Mino, T. M. Loehr, T. E. Meyer, M. A. Cusanovich, W. V. Sweeney, E. T. Adman, and J. Sanders-Loehr. 1991. The environment of the Fe_4S_4 clusters in ferredoxins and high-potential iron proteins. New information from x-ray crystallography and resonance Raman spectroscopy. *J. Am. Chem. Soc.* 113:2055–2064.

Beck, B. W. 1997. Theoretical Investigations of Iron-Sulfur Proteins. Ph.D. thesis. Washington State University, Pullman, WA.

Bernstein, F. C., T. F. Koetzle, G. J. B. Williams, E. F. Meyer, M. D. Brice, J. R. Rodgers, O. Kennard, T. Shimanouchi, and M. Tasumi. 1977. The protein data bank: a computer-based archival file for macromolecular structures. *J. Mol. Biol.* 112:535–542.

Bertini, I., A. Donaire, B. A. Feinberg, C. Luchinat, M. Piccioli, and H. Yuan. 1995. Solution structure of the oxidized 2(4Fe-4S) ferredoxin from *Clostridium pasteurianum. Eur. J. Biochem.* 232:192–205.

Brereton, P. S., F. J. M. Verhagen, Z. H. Zhou, and M. W. W. Adams. 1998. Effect of iron-sulfur cluster environment in modulating the thermodynamic properties and biological function of ferredoxin from *Pyrococcus furiosus. Biochemistry.* 37:7351–7362.

Brooks, B., R. E. Bruccoleri, B. D. Olafson, D. J. States, S. Swaminathan, and M. Karplus. 1983. CHARMM: a program for macromolecular energy, minimization, and dynamics calculations. *J. Comp. Chem.* 4:187–217.

Bryant, D. A. 1992. Molecular biology of photosystem I. *In* The Photosystems: Structure, Function and Molecular Biology. J. Barber, editor. Elsevier Science Publishers, Amersterdam. 501–549.

Busse, S. C., G. N. La Mer, L. P. Yu, J. P. Howard, E. T. Smith, Z. H. Zhou, and M. W. W. Adams. 1992. Proton NMR investigation of the oxidized three-iron clusters in the ferredoxins from the hyperthermophilic archae *Pyrococcus furiosus* and *Thermococcus litoralis. Biochemistry.* 31:11952–11962.

Cammack, R. 1992. Iron-sulfur cluster in enzymes: themes and variations. *In* Iron-Sulfur Proteins. R. Cammack, editor. Academic Press, San Diego. 281–322.

Crespi, H. L., A. G. Kostka, and U. H. Smith. 1974. Proton magnetic resonance observations of hydrogen exchange rates and secondary structure in algal ferredoxins. *Biochem. Biophys. Res. Commun.* 61: 1407–1414.

Dauter, Z., K. S. Wilson, L. C. Sieker, J. Meyer, and J. M. Moulis. 1997. Atomic resolution (0.94 Å) structure of *Clostridium acidurici* ferredoxin. Detailed geometry of [4Fe-4S] clusters in a protein. *Biochemistry.* 36:16065–16073.

Donaire, A., C. M. Gorst, Z. H. Zhou, M. W. W. Adams, and G. N. La Mar. 1994. ^{1}H NMR investigation of the electronic structure of the four-iron ferredoxin from the hyperthermophilic archaeon *Thermococcus litoralis. J. Am. Chem. Soc.* 116:6841–6849.

Duée, E. D., E. Fanchon, J. Vicat, L. C. Sieker, J. Meyer, and J.-M. Moulis. 1994. Refined crystal structure of the 2[4Fe-4S] ferredoxin from *Clostridium acidurici* at 1.84 Å resolution. *J. Mol. Biol.* 243:683–695.

Eidsness, M. K., A. E. Burden, K. A. Richie, D. M. J. Kurtz, R. A. Scott, E. T. Smith, B. Beard, T. Min, and C. Kang. 1999. Modulation of the redox potential of the $Fe(SCys)_4$ site in rubredoxin by the orientation of a peptide dipole. *Biochemistry.* 38:14803–14809.

Fujii, T., Y. Hata, T. Wakagi, N. Tanaka, and T. Oshima. 1996. Novel zinc-binding centre in thermoacidophilic archaeal ferredoxins. *Nat. Struct. Biol.* 3:834–837.

Fukuyama, K., H. Matsubara, T. Tsukihara, and Y. Katsube. 1989. Structure of [4Fe-4S] ferredoxin from *Bacillus thermoproteolyticus* refined at 2.3 Å resolution. *J. Mol. Biol.* 210:383–398.

Fukuyama, K., Y. Nagahara, T. Tsukihara, Y. Katsube, T. Hase, and H. Matsubara. 1988. Tertiary structure of *Bacillus thermoproteolyticus* [4Fe-4S] ferredoxin: evolutionary implications for bacterial ferredoxins. *J. Mol. Biol.* 199:183–193.

Genetics Computer Group. 1994. Program Manual for the Wisconsin Package. Madison, WI.

Golbeck, J. H. 1993a. Shared thematic elements in photochemical reaction centers. *Proc. Natl. Acad. Sci. U.S.A.* 90:1642–1646.

Golbeck, J. H. 1993b. The structure of photosystem I. *Curr. Opin. Struct. Biol.* 3:508–514.

Gunner, M. R., and B. Honig. 1991. Electrostatic control of midpoint potentials in the cytochrome subunit of the *Rhodopseudomonas viridis* reaction center. *Proc. Natl. Acad. Sci. U.S.A.* 88:9151–9155.

Holm, R. H. 1992. Trinuclear cuboidal and heterometallic cubane-type iron-sulfur clusters: new structural and reactivity themes in chemistry and biology. *In* Iron-Sulfur Proteins. R. Cammack, editor. Academic Press, San Diego. 1–72.

Hong, J.-S., and J. C. Rabinowitz. 1970. Immunological properties and conformational differences detected by tritium-hydrogen exchange of clostridial ferredoxins and apoferredoxins. *J. Biol. Chem.* 245: 4995–5000.

Howard, J. B., and D. C. Rees. 1991. Perspectives on non-heme iron protein chemistry. *Adv. Protein Chem.* 42:199–280.

Ichiye, T. 1999. Computational studies of redox potentials of electron transfer proteins. *In* Simulation and Theory of Electrostatic Interactions in Solution. L. R. Pratt, and G. Hummer, editors. AIP, Santa Fe, NM. 431–450.

Iismaa, S. E., A. E. Vázquez, G. M. Jensen, P. J. Stephens, J. N. Butt, F. A. Armstrong, and B. K. Burgess. 1991. Site-directed mutagenesis of *Azotobacter vinelandii* ferredoxin I. *J. Biol. Chem.* 266:21563–21571.

Jensen, G. M., A. Warshel, and P. J. Stephens. 1994. Calculation of the redox potentials of iron-sulfur proteins: the 2-/3-couple of $[Fe_4S^*_4Cys_4]$ clusters in *Peptococcus Aerogenes* ferredoxin, *Azotobacter vinelandii* ferredoxin I, and *Chromatium vinosum* high-potential iron protein. *Biochemistry.* 33:10911–10924.

Kissinger, C. R., L. C. Sieker, E. T. Adman, and L. H. Jensen. 1991. Refined crystal structure of ferredoxin II from *Desulfovibrio gigas* at 1.7 Å. *J. Mol. Biol.* 219:693–715.

Klukas, O., W.-D. Schubert, P. Jordan, N. Krauβ, P. Fromme, H. T. Witt, and W. Saenger. 1999. Photosystem I, an improved model of the stromal subunits of PsaC, PsaD, and PsaE. *J. Biol. Chem.* 274:7351–7360.

Koerner, J. B., and T. Ichiye. 2000. Interactions of the rubredoxin redox site analog $[Fe(SCH_3)_4]^{2-}$ with water: an ab initio quantum chemistry study. *J. Phys. Chem. B.* 104:2424–2431.

Kraulis, P. J. 1991. MOLSCRIPT: a program to produce both detailed and schematic plots of protein structures. *J. Appl. Crystallogr.* 24:946–950.

Krauss, N., W.-D. Schubert, O. Klukas, P. Fromme, H. T. Witt, and W. Saenger. 1996. Photosystem I at 4 Å resolution represents the first structural model of a joint photosynthetic reaction centre and core antenna system. *Nat. Struct. Biol.* 3:965–973.

Libeu, C. A., M. Kukimoto, M. Nishiyama, S. Horinouchi, and E. T. Adman. 1997. Site-directed mutants of pseudoazurin: explanation of increased redox potentials from X-ray structures and from calculation of redox potential differences. *Biochemistry.* 136:13160–13179.

MacKerell, A. D., Jr., D. Bashford, M. Bellot, R. L. Dunbrack, Jr., M. J. Field, S. Fischer, J. Gao, H. Guo, S. Ha, D. Joseph, K. Kuchnir, K. Kuczera, F. T. K. Lau, M. Mattos, S. Michnick, D. T. Nguyen, T. Ngo, B. Prodhom, B. Roux, M. Schlenkrich, J. Smith, R. Stote, J. Straub, J. Wiorkiewicz-Kuczera, and M. Karplus. 1998. All-atom empirical potential for molecular modeling and dynamics studies of proteins. *J. Phys. Chem. B.* 102:3586–3616.

Masepohl, B., M. Kutsche, K.-U. Riedel, M. Schmehl, W. Klipp, and A. Pühler. 1992. Functional analysis of the cysteine motifs in the ferredoxin-like protein FdxN of *Rhizobium melitoti* involved in symbiotic nitrogen fixation. *Mol. Gen. Genet.* 233:33–41.

Matsubara, H., and K. Saeki. 1992. Structural and functional diversity of ferredoxins and related proteins. *In* Iron-Sulfur Proteins. R. Cammack, editor. Academic Press, San Diego. 223–281.

Merritt, E. A., and M. E. P. Murphy. 1994. Raster3D version 2.0: a program for photorealistic molecular graphics. *Acta Crystallogr.* D50: 869–873.

Mouesca, J. M., J. L. Chen, L. Noodleman, D. Bashford, and D. A. Case. 1994. Density functional/Poisson-Boltzmann calculations of redox potentials for iron-sulfur clusters. *J. Am. Chem. Soc.* 116:11898–11914.

Moulis, J.-M., L. C. Sieker, K. S. Wilson, and Z. Dauter. 1996. Crystal structure of the 2[4Fe-4S] ferredoxin from *Chromatium vinosum*: evolutionary and mechanistic inferences for [3/4Fe-4S] ferredoxins. *Protein Sci.* 5:1765–1784.

Nishiyama, M., J. Suzuki, T. Ohnuki, H. C. Chang, S. Horinouchi, S. Turley, E. T. Adman, and T. Beppu. 1992. Site-directed mutagenesis of pseudoazurin from *Alcaligenes faecalis* S-6: Pro80Ala mutant exhibits marked increase in reduction potential. *Protein Eng.* 5:177–184.

Page, C. C., C. C. Moser, X. Chen, and P. L. Dutton. 1999. Natural engineering principles of electron tunnelling in biological oxidation-reduction. *Nature.* 402:47–52.

Saeki, K., K. Tokuda, K. Fukuyama, H. Matsubara, K. Nadanami, M. Go, and S. Itoh. 1996. Site-specific mutagenesis of *Rhodobacter capsulatus* ferredoxin I, FdxN, that functions in nitrogen fixation. *J. Biol. Chem.* 271:31399–31406.

Schipke, C. G., D. B. Goodin, D. E. McRee, and C. D. Stout. 1999. Oxidized and reduced *Azotobacter vinelandii* ferredoxin I at 1.4 Å resolution: conformational change of surface residues without significant change in the $[3Fe\text{-}4S]^{+/0}$ cluster. *Biochemistry.* 38:8228–8239.

Séry, A., D. Houset, L. Serre, J. Bonicel, C. Hatchikian, M. Frey, and M. Roth. 1994. Crystal structure of the ferredoxin I from *Desulfovibrio africanus* at 2.3 Å resolution. *Biochemistry.* 33:15408–15417.

Shenoy, V. S., and T. Ichiye. 1993. Influence of protein flexibility on the redox potential of rubredoxin: energy minimization studies. *Proteins.* 17:152–160.

Soman, J., S. Iismaa, and C. D. Stout. 1991. Crystallographic analysis of two site-directed mutants of *Azotobacter vinelandii* ferredoxin. *J. Biol. Chem.* 266:21558–21562.

Stephens, P. J., D. J. Jollie, and A. Warshel. 1996. Protein control of redox potentials of iron-sulfur proteins. *Chem. Rev.* 96:2491–2513.

Sticht, H., G. Wildegger, D. Bentrop, B. Darimont, R. Sterner, and P. Rosch. 1996. An NMR-derived model for the solution structure of oxidized *Thermotoga maritima* 1[Fe4–S4] ferredoxin. *Eur. J. Biochem.* 237:726–735.

Stout, C. D. 1993. Crystal structures of oxidized and reduced *Azotobacter vinelandii* ferredoxin at pH 8 and 6. *J. Biol. Chem.* 268:25920–25927.

Stout, C. D., E. A. Stura, and D. E. McRee. 1998. Structure of *Azotobacter vinelandii* 7Fe ferredoxin at 1.35 Å resolution and determination of the [Fe-S] bonds with 0.01 Å accuracy. *J. Mol. Biol.* 278:629–639.

Swartz, P. D., B. W. Beck, and T. Ichiye. 1996. Structural origins of redox potentials in Fe-S proteins: electrostatic potentials of crystal structures. *Biophys. J.* 71:2958–2969.

Sweeney, W. V., and J. C. Rabinowitz. 1980. Proteins containing 4Fe-4S clusters: an overview. *Annu. Rev. Biochem.* 49:139–161.

Voet, D., and J. G. Voet. 1990. Biochemistry. John Wiley and Sons, New York.

Xiao, Z., M. J. Maher, M. Cross, C. S. Bond, J. M. Guss, and A. G. Wedd. 2000. Mutation of the surface valine residues 8 and 44 in the rubredoxin from *Clostridium pasteurianum*: solvent access versus structural changes as determinants of reversible potential. *J. Biol. Inorg. Chem.* 5:75–84.